Population Dynamics in a Changing Environment: Random versus Periodic Switching

Ami Taitelbaum,[1,‡] Robert West,[2,‡] Michael Assaf,[1,*] and Mauro Mobilia[2,†]
[1]Racah Institute of Physics, Hebrew University of Jerusalem, Jerusalem 91904, Israel
[2]Department of Applied Mathematics, School of Mathematics, University of Leeds, Leeds LS2 9JT, United Kingdom

(Received 13 February 2020; revised 13 May 2020; accepted 23 June 2020; published 24 July 2020)

Environmental changes greatly influence the evolution of populations. Here, we study the dynamics of a population of two strains, one growing slightly faster than the other, competing for resources in a time-varying binary environment modeled by a carrying capacity switching either *randomly* or *periodically* between states of abundance and scarcity. The population dynamics is characterized by demographic noise (birth and death events) coupled to a varying environment. We elucidate the similarities and differences of the evolution subject to a stochastically and periodically varying environment. Importantly, the population size distribution is generally found to be broader under intermediate and fast random switching than under periodic variations, which results in markedly different asymptotic behaviors between the fixation probability of random and periodic switching. We also determine the detailed conditions under which the fixation probability of the slow strain is maximal.

DOI: 10.1103/PhysRevLett.125.048105

The evolution of natural populations is influenced by varying environmental conditions: the abundance of nutrients, toxins, or external factors like temperature are subject to random and seasonal variations, and have an important impact on population dynamics [1–3].

Several models of a population response to a changing environment assume that external conditions vary either periodically or stochastically in time [4–26]. These external variations are often modeled by taking a binary environment that switches between two states [26–46]. In finite populations, demographic noise (DN) is another form of randomness that can lead to fixation (one species takes over the population [47,48]). DN is strong in small populations and negligible in large ones. Importantly, the evolution of a population composition is often coupled with the dynamics of its size [49–55]. This can lead to coupling between DN and environmental variability (EV), with external factors affecting the population size, which in turn modulates the DN strength. The interplay between EV and DN plays a key role in microbial communities [56–63]: the variations of their composition and size are vital to understand the mechanisms of antimicrobial resistance [26,58], and may lead to population bottlenecks, where new colonies consisting of few individuals are prone to fluctuations [56,59,61–63]. Interactions between microbial communities and environment have also been found to influence cooperative behavior in *Pseudomonas fluorescens* biofilms [60–62]. EV and DN are also important in ecology, e.g., in modeling tropical forests [14–16] and in gene regulatory networks [17,21].

In most studies, there is no interdependence between the fluctuations stemming from DN and EV, with growth rates often assumed to vary independently of the population size [6,7,11–13,17–22,24,27–29,31,36–38,41,43]. Hence, there is as yet no systematic comparison of the dynamics under random and periodic switching: some works report that they lead to similar evolutionary processes while others find differences, see, e.g., Refs. [29,40]. Here, we systematically study the coupled influence of EV and DN on the dynamics of a population, where slow- and fast-growing strains compete for resources subject to a randomly and periodically switching carrying capacity.

A distinctive feature of this model is that it accounts for the stochastic or periodic depletion and recovery of resources via a binary environment, varying with a finite correlation time or period, and the DN and EV coupling, see Fig. 1. This setting is simple enough to enable us to scrutinize whether environmental perturbations of different nature lead to the same dynamics, and includes many features (switching environment, varying population size) that can be tested in controlled microbial experiments [28,52,55,57,63].

To address the fundamental question of evolution under stochastic and deterministic variations, we consider random and periodic environmental switching. This allows us to elucidate the influence of EV on the population size distribution (PSD) and the fixation properties. We analytically show that the PSD is generally broader under intermediate and fast random switching than under periodic variations, leading to markedly different fixation probabilities. We also determine the switching conditions for which the slow strain's fixation probability is maximized.

We consider a well-mixed population of time-fluctuating size $N(t) = N_S(t) + N_F(t)$ consisting of two strains. At time t, $N_S(t)$ individuals are of a slow-growing strain S, corresponding to a fraction $x = N_S/N$ of the population,

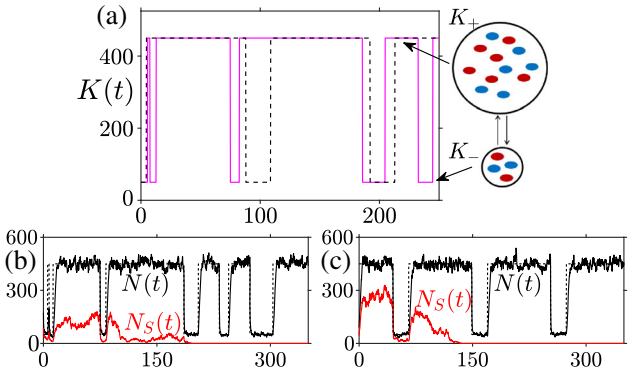

FIG. 1. (a) K versus time t: asymmetric random (pink [light gray] solid) and periodic (black dashed) switching between K_+ and K_- yield fluctuating population composition and size (large and small circles), see text. (b),(c) Typical realizations of N (black), N_S (red [gray]) and K (black dashed) versus t under random (b) and periodic (c) switching: composition changes until fixation occurs. Here $(s, K_0, \nu, \gamma, \delta, x_0) = (0.02, 250, 0.03, 0.8, 0.6, 0.5)$.

and N_F are of a fast-growing species F. The respective per capita growth rates of S and F are $(1-s)/\bar{f}$ and $1/\bar{f}$, which sets the model's timescale [64]. Here, $\bar{f} = (1-s)x + 1 - x = 1 - sx$ is the population average fitness and $0 < s \ll 1$ denotes the small selective growth advantage of F over S [44,45,50,51]. Growth is limited by a logistic death rate N/K, where $K \gg 1$ is the carrying capacity. Population dynamics is often idealized by assuming a static environment (constant K) yielding a constant or logistically varying N [48,69–72]. Here, we instead consider a population of fluctuating size subject to a time-varying environment, and obeying the birth-death process [45,64]: $N_{S/F} \xrightarrow{T^+_{S/F}} N_{S/F} + 1$ and $N_{S/F} \xrightarrow{T^-_{S/F}} N_{S/F} - 1$, with transition rates $T^+_S = (1-s)N_S/\bar{f}$, $T^+_F = N_F/\bar{f}$ and $T^-_{S/F} = (N/K(t))N_{S/F}$. We model EV via a switching carrying capacity

$$K(t) = K_0[1 + \gamma\xi_\alpha(t)], \qquad \xi_\alpha(t) \in \{-1, +1\}, \quad (1)$$

where $K_0 \equiv (K_+ + K_-)/2$ and $\gamma \equiv (K_+ - K_-)/(2K_0)$, while $\alpha \in \{r, p\}$ and $\gamma = \mathcal{O}(1)$. Here, resources vary either randomly ($\alpha = r$) or periodically ($\alpha = p$), between states of scarcity, $K = K_-$ ($\xi_\alpha = -1$), and abundance, $K = K_+$ ($\xi_\alpha = +1$), where $K_+ > K_- \gg 1$, causing fluctuations of population size and composition, see Fig. 1. This specific choice of birth-death process coupled to a time-varying binary environment is arguably the simplest biologically relevant model to study population dynamics under the joint influence of EV and DN, see Section 1.1 in [64].

When $K(t)$ switches randomly, ξ_r is a colored asymmetric dichotomous (telegraph) Markov noise (ADN) [73,74], with the transition $\xi_r \to -\xi_r$ occurring at rate $\nu_\pm$ when $\xi_r = \pm 1$. The (average) switching rate is $\nu = (\nu_+ + \nu_-)/2$ while $\delta = (\nu_- - \nu_+)/(2\nu)$ measures the switching asymmetry ($|\delta| < 1$, with $\delta = 0$ for symmetric switching). In this model, the ADN is a stationary noise of mean $\langle \xi_r(t) \rangle = \delta$ and autocorrelation function $\langle \xi_r(t)\xi_r(t') \rangle - \langle \xi_r(t) \rangle \langle \xi_r(t') \rangle = (1-\delta^2)e^{-2\nu|t-t'|}$ ($\langle \cdot \rangle$ denotes ensemble averaging). When $K(t)$ switches periodically, ξ_p is a rectangular wave defined by the rectangular function, rect$(\cdot)$ [75], of period $T = (1/\nu_+) + (1/\nu_-) = 2/[(1-\delta^2)\nu]$:

$$\xi_p(t) = \sum_{j=-\infty}^{\infty} \left[\text{rect}\left(\frac{t + \frac{1}{2\nu_+} + jT}{1/\nu_+} \right) - \text{rect}\left(\frac{t - \frac{1}{2\nu_-} + jT}{1/\nu_-} \right) \right],$$

which becomes the square wave $\xi_p(t) = -\text{sign}\{\sin(\pi\nu t)\}$ when $\delta = 0$. In our simulations, $\xi_p(t)$ averaged over a period T has the same mean and variance as $\xi_r(t)$. Hence, the mean and variance of $K(t)$ are the same for $\alpha \in \{r, p\}$: $\langle K(t) \rangle = K_0(1 + \gamma\delta)$ and $\text{var}(K) = (\gamma K_0)^2(1-\delta^2)$ [76].

The model considered here gives rise to a long-lived population size distribution (PSD) followed by an eventual extinction of the entire population which occurs after a very long time (practically unobservable when $K_0 \gg 1$ [44] [77]). Below, we focus on intermediate times $t = \mathcal{O}(s^{-1})$, a timescale on which one species is likely to have gone extinct and the other fixated the population that is in its long-lived PSD [64]. We show that the fixation probabilities strongly depend on the PSD that is encoded in the underlying master equation [45,46,78,79], see [64] for details.

Insight into the dynamics is gained by ignoring fluctuations and considering the mean-field picture of a very large population with constant $K = K_0$. Here, N and x evolve according to $dN/dt \equiv \dot{N} = N(1 - N/K_0)$ and $\dot{x} = -sx(1-x)/(1-sx)$ [50,51,64], with x decaying on a timescale $t \sim s^{-1} \gg 1$ and $N(t) = \mathcal{O}(K_0)$ after $t = \mathcal{O}(1)$ [80]. Thus, a timescale separation occurs: the relaxation of x is much slower than that of N.

However, when dealing with a finite population, DN (random birth and death events) must be taken into account, yielding the fixation of one of the species. The S fixation probability, given a fixed population size N, and an initial fraction $x_0 = N_S(0)/N(0)$ of S individuals, is [48,71,79]

$$\phi(x_0)|_N = [e^{-Nx_0\ln(1-s)} - 1]/[e^{-N\ln(1-s)} - 1], \quad (2)$$

which exponentially decreases with N. For $s \ll N^{-1/2} \ll 1$ ("diffusion approximation"), this simplifies to $\phi(x_0)|_N \simeq (e^{-Ns(1-x_0)} - e^{-Ns})/(1 - e^{-Ns})$ [44,45,70]. While Eq. (2) provides a good approximation for the fixation probability also when N fluctuates about constant $K = K_0$, this picture changes drastically when, in addition to DN, the population is subject to a time-varying $K(t)$, see Fig. 1. Below we study the joint influence of EV and DN on the PSD and fixation properties.

Population size distribution.—Simulations show that the marginal quasistationary PSD, $P^{(\alpha)}_\nu(N)$ (unconditioned on

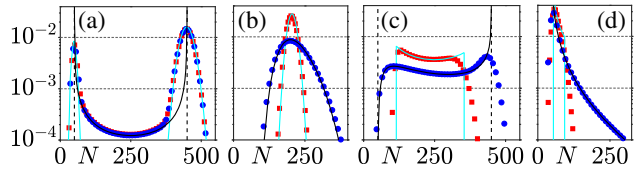

FIG. 2. $P_\nu^{(r)}(N)$ (blue [dark gray]) and $P_\nu^{(p)}(N)$ (red [gray]) for different ν: (a) $\nu = 0.05$, (b) $\nu = 17.5$, (c) $\nu = 1.4$, (d) $\nu = 1$. Symbols are from simulations; solid black lines in (a)–(d) are from P_ν^{PDMP}, those in cyan [light gray] are from $P_0(N)$ in (a), P_ν^{Kap} in (b), and P_ν^{PPP} in (c),(d); vertical dashed lines in (a),(c) show $N = K_\pm$, see text; horizontal dashed lines are eye guides. Here $(s, K_0, \gamma, x_0) = (0.05, 250, 0.8, 0.6)$, $\delta = 0.7$ in (a)–(c) and $\delta = -0.5$ in (d).

ξ_α), is characterized by different regimes depending on the switching rate ν, with markedly different features in the case of random and periodic variations when $\nu = \mathcal{O}(1)$ and $\nu \gg 1$, see Fig. 2.

The case of random switching can be treated as in [44,45] for $\delta = 0$. Upon ignoring DN, $N(t)$ is therefore subject only to ADN according to the piecewise-deterministic Markov process (PDMP) [64,81,82] defined by the stochastic differential equation $\dot{N} = N[1 - (N/\mathcal{K})(1 - \gamma\xi_r)/(1 - \gamma\delta)]$, where $\mathcal{K} \equiv K_0(1 - \gamma^2)/(1 - \gamma\delta)$. When $\nu \to \infty$, the ADN self-averages, $\xi \xrightarrow{\nu\to\infty} \langle\xi\rangle = \delta$, and $N \xrightarrow{\nu\to\infty} \mathcal{K}$. The marginal PSD of this PDMP has support $[K_-, K_+]$ and can be computed explicitly [45,73]: its expression $P_\nu^{\mathrm{PDMP}}(N)$ is given by Eq. (S22) of [64]. Although P_ν^{PDMP} only accounts for EV, when $K_0 \gg 1$ and $\gamma = \mathcal{O}(1)$, it captures the peaks of $P_\nu^{(r)}$ and the average population size, see Figs. 2 and S3(b) [64]. However, P_ν^{PDMP} ignores DN and cannot capture the width of $P_\nu^{(r)}$ about its peaks, see Figs. 2(a), 2(c), and 2(d). Yet, this can be remedied, by a linear noise approximation, see [45] and Section 3.2 in [64]. We can also obtain a PDMP-like approximation (ignoring DN) [74,83] of the periodic PSD by solving the mean-field equation for $N(t)$ with periodic $K(t)$. By inverting $N(t)$ we then obtain the piecewise periodic process (PPP) approximation P_ν^{PPP} of $P_\nu^{(p)}$, given by (S19) in Section 2.3 of [64], which is valid over a broad range of switching rates, see Figs. 2(c) and 2(d) and below.

Furthermore, for periodic switching, the full $P_\nu^{(p)}$ can be found analytically in the limits of very slow ($\nu \to 0$) and fast ($\nu \gg 1$) variations. For $\nu \to 0$ the carrying capacity is initially randomly allocated and almost constant, i.e., $K(t) \simeq K(0)$. The PSD is thus the same for periodic and random switching: $P_0^{(p)} = P_0^{(r)} \equiv P_0$, and can be computed from the master equation. Assuming $K_0 \gg 1$ and $\gamma = \mathcal{O}(1)$, the PSD is bimodal with peaks about $N = K_\pm$, whose intensity depends on δ [64]: $P_0(N) \simeq [(1 + \delta)K_+^{N+1}e^{-K_+} + (1 - \delta)K_-^{N+1}e^{-K_-}]/[2N \cdot N!]$. This result excellently agrees with simulations, see Fig. 2(a). Under fast periodic switching, $P_\nu^{(p)}$ differs markedly from its random counterpart, see Fig. 2(b). An approximate expression of $P_\nu^{(p)}$ to leading order in $1/\nu$, here denoted by P_ν^{Kap}, and peaked at $N = \mathcal{K}$ when $\nu \to \infty$ is given by Eq. (S15) in [64]. P_ν^{Kap} is obtained from the master equation by using the WKB approximation [84] and the Kapitza method [12,24,85], i.e., separating the dynamics into fast and slow variables, see Section 2.2 of [64]. In Fig. 2(b), we notice that both $P_\nu^{(p)} \simeq P_\nu^{\mathrm{Kap}}$ and $P_\nu^{(r)} \simeq P_\nu^{\mathrm{PDMP}}$ are unimodal and peaked about $N \approx \mathcal{K}$ when $\nu \gg 1$, but P_ν^{Kap} is much sharper and narrower than P_ν^{PDMP}. In fact, the variance of P_ν^{PDMP} scales as K_0^2/ν when $1 \ll \nu \ll K_0$, and is much larger than that of P_ν^{Kap}, see Section 4.3 in [64].

Note that while P_0 and P_ν^{Kap} account for DN and EV, P_ν^{PDMP} and P_ν^{PPP} only account for EV. Yet, DN is negligible compared to EV when $1 \lesssim \nu \ll K_0$ and $1 \lesssim \nu \ll \sqrt{K_0}$ in the random and periodic cases, respectively [64]. P_ν^{PDMP} and P_ν^{PPP} are therefore suitable approximations of $P_\nu^{(\alpha)}$ in those regimes.

In particular, P_ν^{PDMP} and P_ν^{PPP} allow us to characterize interesting phenomena arising in the intermediate asymmetric switching regime where $\nu \gtrsim 1$ with $\nu_- > 1$ and $\nu_+ < 1$, or $\nu_- < 1$ and $\nu_+ > 1$, i.e., when $1/(1 + |\delta|) < \nu < 1/(1 - |\delta|)$. In the former case ($\delta > 0$), $P_\nu^{(r)}$ has a peak at $N \approx K_+$ and, under sufficiently strong EV, exhibits also a peak N^* between K_- and K_+ (*i.e.*, $K_- < N^* < K_+$), whose position is aptly captured by P_ν^{PDMP}, see Fig. 2(c) and Section 3.1 in [64]. In Fig. 2(c), $P_\nu^{(p)}$ is less broad than $P_\nu^{(r)}$ and has also two peaks well reproduced by P_ν^{PPP}, whose support is narrower than that of P_ν^{PDMP} [64]. When $\nu \gtrsim 1$, with $\nu_- < 1$ and $\nu_+ > 1$ ($\delta < 0$), $P_\nu^{(r)}$ and $P_\nu^{(p)}$ exhibit a single peak at $N \approx K_-$, well predicted by P_ν^{PDMP} and P_ν^{PPP}, with the latter being narrower than the former, see Fig. 2(d). In fact, Figs. 2(b) and 2(c) show that the transition from bimodal to unimodal PSD (slow to fast switching) is generally more abrupt under periodic than under random switching.

Fixation probability.—We denote by ϕ_α the slow (S) species fixation probability subject to α switching ($\alpha \in \{r, p\}$). As aforementioned, when $s \ll 1$ and $t \gtrsim \mathcal{O}(1)$, the system has settled in its long-lived PSD. Thus, given x_0, ϕ_α can be approximated by averaging $\phi(x_0)|_N$ over $P_{\nu/s}^{(\alpha)}(N)$, upon rescaling $\nu \to \nu/s$ [44,45]

$$\phi_\alpha(\nu) \simeq \int_0^\infty P_{\nu/s}^{(\alpha)}(N)\phi(x_0)|_N dN, \qquad \alpha \in \{r, p\}. \quad (3)$$

This result is valid under weak selection, $1/K_0 \ll s \ll 1$, when there are $\mathcal{O}(\nu/s)$ switches prior to fixation [44,45,64]. The difference between ϕ_r and ϕ_p stems from the different ν dependence of $P_\nu^{(r)}$ and $P_\nu^{(p)}$, see Fig. 2. Approximations of ϕ_r and ϕ_p are obtained by respectively

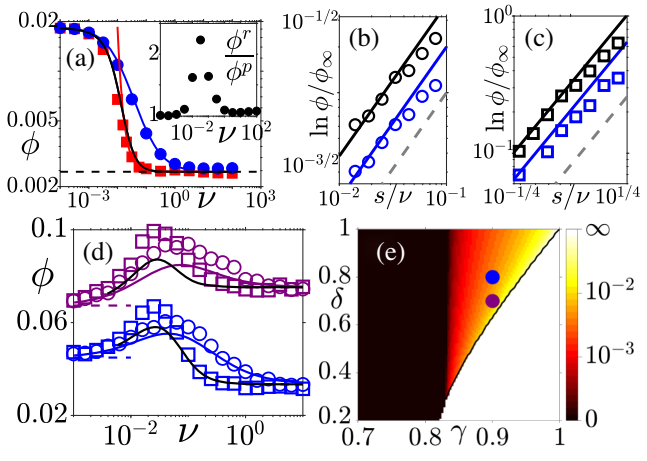

FIG. 3. (a)–(d) fixation probability for random and periodic switching (circles and squares): symbols are from simulations. In (a) solid lines are from (S38) (blue [dark gray], $\alpha = r$), (4) (red [gray], $\alpha = p$), and (S39) (black, $\alpha = p$) of [64]. (a) ϕ_α versus ν with $\delta = 0.2$; dashed line shows $\phi^{(\infty)}$. Inset: ϕ_r/ϕ_p versus ν with $\delta = 0.2$. (b),(c) $\ln(\phi_\alpha/\phi^{(\infty)})$ versus s/ν for random (b) and periodic (c) switching with $\delta = 0.2$ (black) and $\delta = 0$ (blue [dark gray]). Dashed gray lines are eye guides $\propto s/\nu$ in (b) and $\propto (s/\nu)^2$ in (c). (d) Nonmonotonic $\phi_\alpha(\nu)$ with $\delta = 0.7$ (purple [gray]) and $\delta = 0.8$ (blue [dark gray]). Solid lines are from (S38) (purple [gray] and blue [dark gray]) and from (S39) (black) of [64]; dashed lines show $\phi^{(0,\infty)}$. $\phi_r(\nu)$ and $\phi_p(\nu)$ are maximal at $\nu = \nu_r^* \approx 0.1$ and $\nu = \nu_p^* \approx 0.07$, see text. (e) Heatmap of ν_r^* (see Section 5.1 in [64] for details and heatmap of ν_p^*): $\nu_r^* \to 0, \infty$ in the black and white areas, respectively; $\phi_r(\nu)$ is nonmonotonic in the red-yellow [gray] area, with $\nu_r^* \approx 0.01$ (red [gray])–$\nu_r^* \approx 0.1$ (yellow [light gray]), see vertical bar. Symbols are for $\delta = 0.7$ (purple [gray]) and $\delta = 0.8$ (blue [dark gray]). Here $(s, K_0, \gamma, x_0) = (0.025, 800, 0.7, 0.5)$ in (a)–(c) and (0.05,250,0.9,0.6) in (d),(e).

substituting $P_{\nu/s}^{(\alpha)}$ by $P_{\nu/s}^{\mathrm{PDMP}}$ and $P_{\nu/s}^{\mathrm{PPP}}$ into Eq. (3). This yields expressions (S38) and (S39) of [64] which are valid over a broad range of ν [44,64], see Figs. 3 and S2(c) and S2(d) [64]. Notably, when $\nu/s \gg 1$, ϕ_p is better approximated by substituting $P_{\nu/s}^{(p)}$ by $P_{\nu/s}^{\mathrm{Kap}}$ in Eq. (3), see below and [64].

When $\nu \to 0$ (slow switching), on average there are almost no switches prior to fixation and $P_{\nu/s}^{(\alpha)}$ is peaked at $N = K_\pm$. Hence, with Eq. (3), $\lim_{\nu\to 0}\phi_\alpha(\nu) \simeq \phi^{(0)} = [(1-\delta)\phi(x_0)|_{K_-} + (1+\delta)\phi(x_0)|_{K_+}]/2$. Figure 3(d) confirms that ϕ_r and ϕ_p approach $\phi^{(0)}$ when $\nu/s \ll 1$.

When $\nu/s \gg 1$ (fast switching), $P_{\nu/s}^{(\alpha)}$ is sharply peaked at $N \simeq \mathcal{K}$, see Fig. 2(b), and to leading order $\lim_{\nu\to\infty}\phi_\alpha(\nu) \simeq \phi^{(\infty)} = \phi(x_0)|_{\mathcal{K}}$ [44,45]. Simulation results of Fig. 3 confirm that at $\nu \gg s$, $\phi_r(\nu)$ and $\phi_p(\nu)$ converge to $\phi^{(\infty)}$. Thus, the fixation probability under fast random or periodic switching is the same to lowest order in $1/\nu$. Yet, the rate of convergence differs, see Fig. 3(a). This is explained by computing the next-to-leading order of ϕ_α in $\nu/s \gg 1$. For this, we use Eq. (3) with Eq. (2) and $P_{\nu/s}^{\mathrm{PDMP}}$ and $P_{\nu/s}^{\mathrm{Kap}}$ for random and periodic switching, respectively. A saddle point calculation, with $1/K_0 \ll s \ll 1$, yields (see Section 4 in [64])

$$\ln\left(\frac{\phi_\alpha(\nu)}{\phi^{(\infty)}}\right) \simeq \begin{cases} \mathcal{A}_r(s/\nu) & (\alpha = r), \\ \mathcal{A}_p(s/\nu)^2 & (\alpha = p). \end{cases} \tag{4}$$

Here $\phi^{(\infty)} = e^{m/2}$, $m \equiv 2\mathcal{K}(1-x_0)\ln(1-s)$, and $\mathcal{A}_r = m(4+m)(1-\delta^2)[\gamma/(1-\gamma\delta)]^2/16$ while $\mathcal{A}_p = \mathcal{K}[1-(1+m/\mathcal{K})^3][\gamma/(1-\gamma\delta)]^2/72$. Thus, when $K_0 s \gg 1$, $\phi_\alpha(\nu)$ converges to $\phi^{(\infty)}$ much faster in the periodic than in the random case, see Figs. 3(a)–(c). The different asymptotic behavior can be understood by noting that $P_\nu^{(r)}$ is generally broader than $P_\nu^{(p)}$, with respective variances scaling as ν^{-1} and ν^{-2}. N can thus attain smaller values under random than periodic switching, which enhances ϕ_r with respect to ϕ_p [86]. When $\nu/s \gg 1$, $\phi_{r,p}$ is determined by the mean $\langle N\rangle \simeq \mathcal{K}$ of $P_\nu^{(\alpha)}$, and the different rate of convergence to $\phi^{(\infty)}$ stems from the deviations of $\langle N\rangle$ from $\mathcal{K}$, which decrease as ν^{-1} when $\alpha = r$ and ν^{-2} when $\alpha = p$, see Section 4.3 in [64]. Another signature of the different asymptotic behavior is the sharp peak of the ratio ϕ_r/ϕ_p at a nontrivial ν, see Fig. 3 (a, inset).

Under intermediate (rescaled) switching, ϕ_α exhibits a rich behavior, see Fig. 3(d). When the switching asymmetry is sufficiently large, ϕ_α is a nonmonotonic function of ν in a nontrivial region $\gamma > \gamma_c(s)$, $\delta > \delta_c(\gamma, s)$ of the parameter space that can be found from Eq. (3), see Figs. 3(d) and 3(e) and Section 5.1 in [64]. The PDMP- and PPP-based approximations [Eqs. (S38) and (S39) in [64]] adequately capture the ν dependence of ϕ_α in this regime, and its maximum at $\nu_\alpha^* \sim s$. This optimal switching rate, which maximizes the S species fixation probability at given (γ, δ, s), corresponds to $\mathcal{O}(1)$ switches prior to fixation. The relative increase in $\phi_\alpha(\nu)$, given by $\phi_\alpha(\nu_\alpha^*)/\max(\phi^{(0)}, \phi^{(\infty)}) - 1$ reaches up to 30%, see Figs. 3(d) and 3(e). In agreement with the PDMP- and PPP-based approximations, we find that $\nu_p^* \lesssim \nu_r^*$, and $\phi_p(\nu_p^*)$ is narrower around the peak than $\phi_r(\nu_r^*)$, see Figs. 3(d) and 3(e) and S2(e) [64]. When the asymmetry is not too large ($|\delta| < \delta_c$), $\phi_\alpha(\nu)$ is a monotonic function: it increases (decreases) with ν below (above) a critical selection intensity s_c (with γ, δ fixed), see Section 5.2 and Fig. S2(d) in [64]. Remarkably, transitions between monotonic and nonmonotonic behavior of $\phi_\alpha(\nu)$ are also found when S produces public goods benefiting the entire population, see Section 7 in [64].

Inspired by the evolution of microbial communities in fluctuating environments, we have studied the dynamics of a population of two strains competing for resources subject

to a binary carrying capacity, switching randomly or periodically in time. We have analyzed how the coupling of demographic noise and environmental variability affects the population size and fixation properties. We have shown that the population size distribution is generally broader under random variations than under periodic changes in the intermediate or fast switching regime, which lead to markedly different asymptotic behaviors of the fixation probabilities. We have also determined the conditions under which the probability that the slow species prevails is maximal. Our work sheds light on the similarities and differences of evolution in stochastically versus deterministically varying environments, and is thus relevant to microbial communities, often subject to frequent and extreme environmental changes.

We are grateful to E. Frey, A. M. Rucklidge, and K. Wienand for useful discussions. A. T. and M. A. acknowledge support from the Israel Science Foundation Grant No. 300/14 and the United States-Israel Binational Science Foundation Grant No. 2016-655. The support of an EPSRC Ph.D. studentship to RW (Grant No. EP/N509681/1) is also gratefully acknowledged.

*michael.assaf@mail.huji.ac.il
†M.Mobilia@leeds.ac.uk
‡Equally contributed to this work.

[1] C. R. Morley, J. A. Trofymow, D. C. Coleman, and C. Cambardella, Microbiol. Ecol. **9**, 329 (1983).
[2] C. A. Fux, J. W. Costerton, P. S. Stewart, and P. Stoodley, Trends Microbiol. **13**, 34 (2005).
[3] Caporaso *et al.*, Genome Biol. **12**, R50 (2011).
[4] H. Beaumont, J. Gallie, C. Kost, G. Ferguson, and P. Rainey, Nature (London) **462**, 90 (2009).
[5] P. Visco, R. J. Allen, S. N. Majumdar, and M. R. Evans, Biophys. J. **98**, 1099 (2010).
[6] R. M. May, *Stability and Complexity in Model Ecosystems* (Princeton University Press, Princeton, USA, 1973).
[7] S. Karlin and B. Levikson, Theor. Popul. Biol. **6**, 383 (1974).
[8] P. L. Chesson and R. R. Warner, Am. Nat. **117**, 923 (1981).
[9] M. Loreau and C. de Mazancourt, Am. Nat. **172**, E49 (2008).
[10] B. K. Xue and S. Leibler, Phys. Rev. Lett. **119**, 108103 (2017).
[11] E. Kussell and S. Leibler, Science **309**, 2075 (2005).
[12] M. Assaf, A. Kamenev, and B. Meerson, Phys. Rev. E **78**, 041123 (2008).
[13] M. Assaf, A. Kamenev, and B. Meerson, Phys. Rev. E **79**, 011127 (2009).
[14] R. A. Chisholm *et al.*, Ecol. Lett. **17**, 855 (2014).
[15] D. A. Kessler and N. Shnerb, J. Theor. Biol. **345**, 1 (2014).
[16] M. Kalyuzhny, R. Kadmon, and N. M. Shnerb, Ecol. Lett. **18**, 572 (2015).
[17] M. Assaf, E. Roberts, Z. Luthey-Schulten, and N. Goldenfeld, Phys. Rev. Lett. **111**, 058102 (2013).
[18] Q. He, M.Mobilia, and U. C. Täuber, Phys. Rev. E **82**, 051909 (2010).
[19] U. Dobramysl and U. C. Täuber, Phys. Rev. Lett. **110**, 048105 (2013).
[20] M. Assaf, M. Mobilia, and E. Roberts, Phys. Rev. Lett. **111**, 238101 (2013).
[21] E. Roberts, S. Be'er, C. Bohrer, R. Sharma, and M. Assaf, Phys. Rev. E **92**, 062717 (2015).
[22] A. Melbinger and M. Vergassola, Sci. Rep. **5**, 15211 (2015).
[23] M. Assaf and B. Meerson, J. Phys. A **50**, 263001 (2017).
[24] O. Vilk and M. Assaf, Phys. Rev. E **97**, 062114 (2018).
[25] U. Dobramysl, M. Mobilia, M. Pleimling, and U. C. Täuber, J. Phys. A **51**, 063001 (2018).
[26] L. Marrec and A.-F. Bitbol, PLoS Comput. Biol. **16**, e1007798 (2020).
[27] E. Kussell, R. Kishony, N. Q. Balaban, and S. Leibler, Genetics **169**, 1807 (2005).
[28] M. Acar, J. Mettetal, and A. van Oudenaarden, Nat. Genet. **40**, 471 (2008).
[29] M. Thattai and A. van Oudenaarden, Genetics **167**, 523 (2004).
[30] S. P. Otto and M. C. Whitlock, Genetics **146**, 723 (1997), http://www.genetics.org/content/146/2/723.
[31] B. Gaál, J. W. Pitchford, and A. J. Wood, Genetics **184**, 1113 (2010).
[32] K. Wienand, M.Sc. thesis, Ludwig-Maximilians-Universität München, 2011.
[33] P. Patra and S. Klumpp, PLoS One **8**, e62814 (2013).
[34] P. Patra and S. Klumpp, Phys. Biol. **12**, 046004 (2015).
[35] E. A. Yurtsev, H. X. Chao, M. S. Datta, T. Artemova, and J. Gore, Mol. Syst. Biol. **9**, 683 (2013).
[36] P. Ashcroft, P. M. Altrock, and T. Galla, J. R. Soc. Interface **11**, 20140663 (2014).
[37] M. Danino and N. M. Shnerb, J. Theor. Biol. **441**, 84 (2018).
[38] P. G. Hufton, Y. T. Lin, and T. Galla, J. Stat. Mech. (2018) 023501.
[39] Q. Su, A. McAvoy, L. Wang, and M. A. Nowak, Proc. Natl. Acad. Sci. U.S.A. **116**, 25398 (2019).
[40] I. Meyer and N. M. Shnerb, arXiv:1912.06386.
[41] P. G. Hufton, Y. T. Lin, T. Galla, and A. J. McKane, Phys. Rev. E **93**, 052119 (2016).
[42] J. Hidalgo, S. Suweis, and A. Maritan, J. Theor. Biol. **413**, 1 (2017).
[43] R. West, M. Mobilia, and A. M. Rucklidge, Phys. Rev. E **97**, 022406 (2018).
[44] K. Wienand, E. Frey, and M. Mobilia, Phys. Rev. Lett **119**, 158301 (2017).
[45] K. Wienand, E. Frey, and M. Mobilia, J. R. Soc. Interface **15**, 20180343 (2018).
[46] R. West and M. Mobilia, J. Theor. Biol. **491**, 110135 (2020).
[47] J. F. Crow and M. Kimura, *An Introduction to Population Genetics Theory* (Blackburn Press, New Jersey, 2009).
[48] W. J. Ewens, *Mathematical Population Genetics* (Springer, New York, 2004).
[49] J. Roughgarden, *Theory of Population Genetics and Evolutionary Ecology: An Introduction* (Macmillan, New York, 1979).
[50] A. Melbinger, J. Cremer, and E. Frey, Phys. Rev. Lett. **105**, 178101 (2010).

[51] J. Cremer, A. Melbinger, and E. Frey, Phys. Rev. E **84**, 051921 (2011).
[52] J. Cremer, A. Melbinger, and E. Frey, Sci. Rep. **2**, 281 (2012).
[53] A. Melbinger, J. Cremer, and E. Frey, J. R. Soc. Interface **12**, 20150171 (2015).
[54] C. S. Gokhale and C. Hauert, Theor. Popul. Biol. **111**, 28 (2016).
[55] J. S. Chuang, O. Rivoire, and S. Leibler, Science **323**, 272 (2009).
[56] L. M. Wahl, P. J. Gerrish, and I. Saika-Voivod, Genetics **162**, 961 (2002), http://www.genetics.org/content/162/2/961.
[57] K. Wienand, M. Lechner, F. Becker, H. Jung, and E. Frey, PLoS One **10**, e0134300 (2015).
[58] J. Coates, B. R. Park, D. Le, E. Şimşek, W. Chaudhry, and M. Kim, eLife **7**, e32976 (2018).
[59] Z. Patwas and L. M. Wahl, Evolution **64**, 1166 (2009).
[60] P. B. Rainey and K. Rainey, Nature (London) **425**, 72 (2003).
[61] M. A. Brockhurst, A. Buckling, and A. Gardner, Curr. Biol. **17**, 761 (2007).
[62] M. A. Brockhurst, PLoS One **2**, e634 (2007).
[63] J. Cremer, A. Melbinger, K. Wienand, T. Henriquez, H. Jung, and E. Frey, arXiv:1909.11338.
[64] See the Supplemental Material at http://link.aps.org/supplemental/10.1103/PhysRevLett.125.048105 for information about the model, the simulations, the PSD, Eq. (4), details about Fig. 3, the mean fixation time, and the generalization to a public good scenario, which includes Refs. [65–68]; also available at https://figshare.com/articles/Supplementary_Material/12613370 with additional supporting resources, including videos illustrating Figures 2, 3(a), S1 and S4.
[65] D. T. Gillespie, J. Comput. Phys. **22**, 403 (1976).
[66] D. F. Anderson, J. Chem. Phys. **127**, 214107 (2007).
[67] M. Dykman, E. Mori, J. Ross, and P. Hunt, J. Chem. Phys. **100**, 5735 (1994).
[68] C. M. Bender and S. A. Orszag, *Advanced Mathematical Methods for Scientists and Engineers* (Springer, New York, 1999).
[69] P. A. P. Moran, *The Statistical Processes of Evolutionary Theory* (Clarendon, Oxford, 1962).
[70] R. A. Blythe and A. J. McKane, J. Stat. Mech. (2007) P07018.
[71] T. Antal and I. Scheuring, Bull. Math. Biol. **68**, 1923 (2006).
[72] R. M. Nowak, *Evolutionary Dynamics* (Belknap Press, Cambridge, USA, 2006).
[73] W. Horsthemke and R. Lefever, *Noise-Induced Transitions* (Springer, Berlin, 2006).
[74] I. Bena, Int. J. Mod. Phys. B **20**, 2825 (2006).
[75] A rectangular function is defined as follows: $\mathrm{rect}(x) = 1$ if $|x| < 1/2$, $\mathrm{rect}(x) = 0$ if $|x| > 1/2$, while $\mathrm{rect}(\pm 1/2) = 0$.
[76] Here, $\langle\cdot\rangle$ is the ensemble average in the case of random switching ($\alpha = r$), and the average obtained by integrating over T, i.e., $\langle K(t)\rangle = (1/T)\int_t^{t+T} K(\tau)d\tau$ under periodic switching.
[77] After the extinction of one species, the other has a logistic-like dynamics, see text, with a mean time to extinction scaling exponentially with its carrying capacity [23,78].
[78] M. Assaf and B. Meerson, Phys. Rev. E **81**, 021116 (2010).
[79] S. Redner, *A Guide to First-Passage Processes* (Cambridge Univesity Press, New York, 2001).
[80] When N and x are not coupled and $s \ll 1$, the initial condition $N(0)$ is here irrelevant. We set $N(0) = K_0$ or $N(0) = K_0(1-\gamma^2)/(1-\gamma\delta) = \mathcal{K}$ and confirmed that our results were independent of $N(0)$.
[81] K. Kitahara, W. Horsthemke, and R. Lefever, Phys. Lett. **70A**, 377 (1979).
[82] M. H. A. Davis, J. R. Stat. Soc. Ser. B **46**, 353 (1984).
[83] C. R. Doering and W. Horsthemke, J. Stat. Phys. **38**, 763 (1985).
[84] V. Elgart and A. Kamenev, Phys. Rev. E **70**, 041106 (2004).
[85] L. D. Landau and E. M. Lifshitz, *Mechanics* (Pergamon, Oxford, 1976).
[86] This occurs for $s > s_c$ (generic case), when $\phi_\alpha(\nu)$ is a decreasing monotonic function. On the other hand, $\phi_r \lesssim \phi_p$ when $s < s_c$, $\gamma < \gamma_c$ and $\delta < \delta_c$, see below and Section 5.2 in Ref. [64].